Inverse Problems and Imaging
Volume X, No. 0X, 200X, X–XX

Web site: http://www.aimSciences.org

NEAR-FIELD IMAGING OF THE SURFACE DISPLACEMENT ON AN INFINITE GROUND PLANE

Gang Bao

Department of Mathematics, Zhejiang University, Hangzhou, China;
and Department of Mathematics, Michigan State University, East Lansing, MI 48824, USA.

Junshan Lin

Institute for Mathematics and its Applications, University of Minnesota, Minneapolis, MN 55455, USA

(Communicated by Haomin Zhou)

Abstract. This paper is concerned with the inverse diffraction problem for an unbounded obstacle which is a ground plane with some local disturbance. The data is collected in the near-field regime with a distance above the surface displacement that is smaller than the wavelength. In this regime, the evanescent modes carried by the scattered wave are significant, which makes it different from the far-field measurement. We formulate explicitly the connection between the evanescent wave modes and the high frequency components of the surface displacement, and present a new numerical scheme to reconstruct the surface displacement from the boundary measurements. By extracting the information carried by the evanescent modes effectively, it is shown that the resolution of the reconstructed image is significantly improved in the near field. Numerical examples show that images with a resolution of $\lambda/10$ are obtained.

1. Introduction

There has been much interest in the near-field optics in the past two decades, in particular motivated by applications in the near-field microscopy. The study of the near-field optics has its origin in an effort to break the diffraction limit imposed by the far-field imaging, where only the propagating wave components with spatial frequency below the wavenumber are available, and the resolution of the image is approximately $\lambda/2$ [4, 15, 16]. In the near field, however, the bandwidth of the spatial frequency may be expanded by taking account of the evanescent (exponentially decayed) waves. We refer the reader to [3, 5, 8, 18] and the references therein for detailed discussions when single scattering (or Born approximation) is assumed.

In this paper, we consider the full scattering of the time harmonic electromagnetic wave that impinges on an infinite ground (x_1x_3) plane with some local disturbance. We focus the study on the TM polarization or E-parallel case, and assume that the surface displacement is invariant along the x_3 direction. Consequently, the Maxwell equations are reduced to the two dimensional Helmholtz equation.

2000 *Mathematics Subject Classification:* 35J05, 35R30, 65N21.

Key words and phrases: inverse scattering,near-field imaging, Helmholtz equation.

G Bao's research was supported in part by the NSF grants DMS-0908325, CCF-0830161, EAR-0724527, DMS-0968360, DMS-1211292, the ONR grant N00014-12-1-0319, a Key Project of the Major Research Plan of NSFC (No. 91130004), and a special research grant from Zhejiang University.

©200X AIMSciences

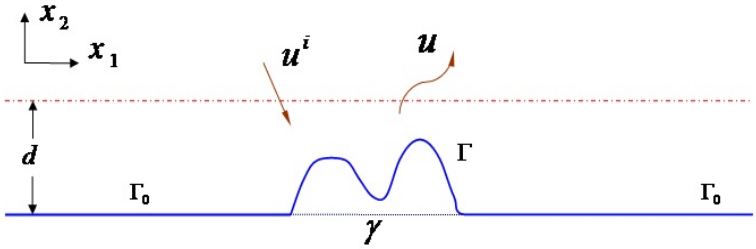

FIGURE 1. Setup of the problem.

Before introducing the forward scattering model, we describe the geometry of the obstacle shown in Figure 1. Let $\gamma \subset \mathbb{R}$ be bounded, open, and $\partial\gamma$ be the boundary of γ. Denote the closure of γ as $\overline{\gamma}$. The ground plane $\Gamma_0 := \mathbb{R}\backslash\gamma$, and the local surface displacement is represented by $\Gamma := \{x = (x_1, x_2) \mid x_1 \in \gamma,\ x_2 = f(x_1)\}$, where the function f is defined on $\overline{\gamma}$:

$$f(x_1) > 0 \text{ for } x_1 \in \gamma, \quad f(x_1) = 0 \text{ for } x_1 \in \partial\gamma.$$

By requiring $f > 0$ on γ, the surface displacement is directed upward. Clearly, $\partial D := \Gamma \cup \Gamma_0$ is the boundary of the whole unbounded obstacle on which the electromagnetic wave impinges. The domain above ∂D is denoted as D ($\subset \mathbb{R}^2$).

The incident wave field $u^i = e^{ikq\cdot x}$ is a plane wave that propagates along the direction $q = (\sin\theta,\ -\cos\theta)^T$, where θ is the incident angle and $k = \frac{\omega}{c}$ is the wavenumber. Here ω is the angular frequency, and c is the speed of the wave propagating in the vacuum. We also denote the wavelength by λ. If the obstacle is a flat perfect conductor, then the reflected field $u^r = -e^{ikq'\cdot x}$ produced by the flat surface is a plane wave propagating along the direction $q' = (\sin\theta,\ \cos\theta)^T$. In general, the total field u^t from the scattering by $\Gamma \cup \Gamma_0$ consists of three parts: the incident wave u^i, the reflected wave u^r, and the scattered field. The scattered field u satisfies the Helmholtz equation

$$\Delta u + k^2 u = 0 \quad \text{in } D. \tag{1}$$

Assuming that the obstacle is a perfect conductor, the total field vanishes on the boundary. Hence

$$u = -(u^i + u^r) \quad \text{on } \partial D. \tag{2}$$

It is easily seen that $u = 0$ on Γ_0. Moreover, the scattered field satisfies the Sommerfield radiation condition:

$$\lim_{r\to\infty} \sqrt{r}\left(\frac{\partial u}{\partial r} - iku\right) = 0, \quad r = |x|\,. \tag{3}$$

The forward scattering problem (1)-(3) admits a unique solution $u \in C^2(D)\cap C(\bar{D})$ if ∂D is C^2 and boundary data $u|_{\partial D}$ is continuous [20]. Clearly here the plane wave $u^i,\ u^r \in C^\infty(\mathbb{R}^2)$. It is worth mentioning that there are many results on related scattering problems in the literature. The well-posedness of the scattering problem for an obstacle with locally downward surface displacement ($f(x_1) < 0$ for $x_1 \in \gamma$) was studied in [1, 2]. There are also general studies on the scattering by a non-local perturbed half plane. See for example [17, 21] and the references therein.

Our goal of this paper is to study the inverse problem, more specifically near-field imaging of the local surface displacement. In our framework, data is collected on

the line $x_2 = d$ above the surface displacement with a distance that is smaller than the wavelength λ (near-field regime). To be more precise, it is required that $0 < d - \max_{x_1 \in \bar{\gamma}} f(x_1) < \lambda$. The inverse problem is to reconstruct f from the scattered field $u(\cdot, d)$ collected on the line $x_2 = d$. Our work is originally motivated by the recent paper [9], in which a linearized model has been introduced for the nonlinear inverse scattering problem by the single scattering assumption. The authors also proposed a broadband imaging strategy for denoising and improving the resolution of the image. However, this linearized model is valid only if $\frac{f}{\lambda} \ll 1$ and the modulus of its derivative $|f'| \ll 1$ simultaneously. Here we investigate the more general case by considering the full scattering model, for which the linearized model in [9] is no longer valid.

This imaging problem shares many of the well-known difficulties with other inverse boundary value problems, particularly nonlinearity and ill-posedness. However, by collecting data in the near-field regime, the evanescent wave modes which are not accessible in the far-field regime ($d - \max f \gg \lambda$) become significant. This crucial fact may be confirmed by the analysis of the scattered field in Section 2. Evanescent wave modes make it possible to break the diffraction limit. It is shown that such exponentially decayed modes of the scattered wave contain exactly the high spatial frequency information (fine features) of the profile f. Our study in this paper is to analyze the scattered field carefully, and design a numerical method that makes use of the evanescent modes effectively, thus to improve the resolution of the image. Numerical examples confirm that a resolution of $\lambda/10$ is obtained in the near field.

It should be pointed out that our work is different from the reconstruction of the star-like local disturbance by the far-field pattern in [13]. The main focus in the near-field imaging is to break the diffraction limit. In this paper the evanescent wave modes in the near-field regime are studied carefully, and a clear characterization of the connection between the high frequency components of the surface displacement and the evanescent wave modes is given explicitly ((13) in Section 2). The analysis leads naturally to a reconstruction method which extracts the information carried by the evanescent modes effectively and is very different from the far-field reconstruction in [13]. Moreover, we do not impose any restriction on the parameterization of the local surface displacement.

The rest of the paper is organized as follows. Section 2 begins with a brief discussion on the layer potential and boundary integral equations. The scattered field is studied in the near-field regime. In particular, it is shown that the evanescent wave modes are significant in this regime and contain the high spatial frequency information of the profile f. Based on the analysis in Section 2, a reconstruction method is proposed in Section 3. Several numerical examples are presented in Section 4 to demonstrate that the resolution via near-field imaging may be significantly improved compared to the far-field case. The paper is concluded with some general remarks in Section 5.

2. Analysis of the scattered wave

2.1. Layer potential and boundary integral equations.

The boundary integral equation methods have become very popular in recent decades for the simulation of the scattering from an obstacle, and the theory is now very well developed [6, 7]. We begins with a brief discussion in this section before examining the scattered wave in the near-field regime.

Introduce Green's function

$$G(x,y) := \Phi(x,y) - \Phi(x_r,y),$$

where $\Phi(x,y) = \dfrac{i}{4}H_0^{(1)}(k|x-y|)$ is the fundamental solution for the Helmholtz equation in $\mathbb{R}^2$ and x_r is the reflection of x by the x_1 axis, i.e., $x_r = (x_1,-x_2)$.

Denote $\overline{\Gamma} = \Gamma \cup \partial\gamma$, $\Gamma_r := \{\ (x_1,-x_2) \mid x \in \Gamma\ \}$, $\overline{\Gamma \cup \Gamma_r} = \Gamma \cup \Gamma_r \cup \partial\gamma$, and $D_r := \{\ (x_1,-x_2) \mid x \in D\ \}$. For a function $\psi \in C(\overline{\Gamma})$, we define the single layer potential:

$$u(x) \quad = \quad \int_{\overline{\Gamma}} G(x,y)\psi(y)ds_y, \quad x \in \mathbb{R}^2 \backslash \overline{\Gamma \cup \Gamma_r}.$$

The following lemma is concerned with the limit of the normal derivative of the single layer potential, when it is extended from above and below the boundary Γ. The limit for the case when Γ is the smooth boundary of a bounded obstacle is well known [6, 7]. Here Γ is not a closed curve. For completeness, the proof of this lemma is provided in the Appendix A.

Lemma 2.1. *Assume that Γ is C^2. For the single layer potential with continuous density ψ, the following holds:*

$$\left(\frac{\partial u}{\partial \nu}\right)_{\pm}(x) = \int_{\overline{\Gamma}} \frac{\partial G(x,y)}{\partial \nu_x}\psi(y)ds_y \mp \frac{1}{2}\psi(x), \quad x \in \Gamma,$$

where ν is the unit normal directed into D, $\left(\dfrac{\partial u}{\partial \nu}\right)_{\pm}(x) := lim_{h\to 0+}\nu(x)\cdot\nabla u(x \pm h\nu(x))$.

The following representation result may serve as a starting point for the analysis of the scattered field.

Lemma 2.2. *If ∂D is C^3, then there exists $\psi \in C(\overline{\Gamma})$ such that the solution to (1)-(3) can be expressed as the single layer potential*

$$u(x) = \int_{\overline{\Gamma}} G(x,y)\psi(y)ds_y \qquad x \in D. \tag{1}$$

Proof. Let u be the solution of (1)-(3). Note $u = 0$ on Γ_0, by Green's theorem and the radiation condition, the scattered field takes the following form

$$u(x) = \int_{\overline{\Gamma}} \frac{\partial G(x,y)}{\partial \nu_y}u(y) - G(x,y)\frac{\partial u(y)}{\partial \nu_y}ds_y, \quad x \in D. \tag{2}$$

Denote the domain bounded by $\overline{\Gamma \cup \Gamma_r}$ as $\tilde{D}$. Let $u_0 := u^i + u^r$. Then $u_0 \in C^\infty(\mathbb{R}^2)$ satisfies the Helmholtz equation in $\tilde{D}$. By Green's theorem, we have

$$\left(\int_{\overline{\Gamma}} + \int_{\overline{\Gamma}_r}\right)\left(\frac{\partial \Phi(x,y)}{\partial \nu_y}u_0(y) - \Phi(x,y)\frac{\partial u_0(y)}{\partial \nu_y}\right)ds_y = 0, \quad x \in D, \tag{3}$$

where ν_y is the unit normal directed to D for $y \in \overline{\Gamma}$, ν_y is the unit normal directed to D_r for $y \in \overline{\Gamma}_r$.

By noting that $u_0(y) = -u_0(y_r)$, and $\dfrac{\partial u_0(y)}{\partial \nu_y} = -\dfrac{\partial u_0(y_r)}{\partial \nu_{y_r}}$ for $y \in \overline{\Gamma}$, we get

$$\begin{aligned} \int_{\overline{\Gamma}_r} \frac{\partial \Phi(x,y)}{\partial \nu_y} u_0(y) ds_y &= \int_{\overline{\Gamma}} \frac{\partial \Phi(x_r,y)}{\partial \nu_y}(-u_0(y)) ds_y, \\ \int_{\overline{\Gamma}_r} \Phi(x,y) \frac{\partial u_0(y)}{\partial \nu_y} ds_y &= \int_{\overline{\Gamma}} \Phi(x_r,y)(-\frac{\partial u_0(y)}{\partial \nu_y}) ds_y. \end{aligned} \tag{4}$$

Substituting (4) into (3) yields

$$\int_{\overline{\Gamma}} \frac{\partial G(x,y)}{\partial \nu_y} u_0(y) - G(x,y) \frac{\partial u_0(y)}{\partial \nu_y} ds_y = 0, \quad x \in D. \tag{5}$$

A combination of (2) and (5) leads to

$$\begin{aligned} u(x) &= \int_{\overline{\Gamma}} \frac{\partial G(x,y)}{\partial \nu_y}(u+u_0)(y) - G(x,y) \left(\frac{\partial u}{\partial \nu_y} + \frac{\partial u_0}{\partial \nu_y} \right)(y) ds_y, \\ &= -\int_{\overline{\Gamma}} G(x,y) \left(\frac{\partial u}{\partial \nu_y} + \frac{\partial u_0}{\partial \nu_y} \right)(y) ds_y. \quad x \in D. \end{aligned}$$

Let $\psi = -\left(\dfrac{\partial u}{\partial \nu_y} + \dfrac{\partial u_0}{\partial \nu_y} \right)$. $\psi \in C(\overline{\Gamma})$ follows by the standard regularization theory for second-order elliptic equations and the Sobolev imbedding theorems [11]. The proof is now complete.

□

Define the integral operator $K : C(\overline{\Gamma}) \to C(\overline{\Gamma})$ by letting

$$(K\psi)(x) := \int_{\overline{\Gamma}} G(x,y)\psi(y) ds_y, \quad x \in \overline{\Gamma}. \tag{6}$$

Denote $g = -(u^i + u^r)|_{\overline{\Gamma}}$. Then the existence of the solution to the integral equation $K\psi = g$ follows from Lemma 2.2. Note that since the single layer potential can be continuously extended to $\overline{\Gamma}$, the density function ψ defined in Lemma 2.2 is a solution of the integral equation $K\psi = g$. Regarding the uniqueness, the following result holds.

Proposition 1. *If ∂D is C^3, then $K\psi = g$ is uniquely solvable if k^2 is not the eigenvalue of $-\Delta$ in $\tilde{D}$ for the Dirichlet problem. Here $\tilde{D}$ is the domain bounded by $\overline{\Gamma \cup \Gamma_r}$.*

For completeness, we sketch the proof here. If $K\psi = 0$ for some $\psi \in C(\overline{\Gamma})$, then the single layer potential

$$u(x) = \int_{\overline{\Gamma}} G(x,y)\psi(y) ds_y$$

solves the exterior problem

$$\begin{cases} \Delta u_1 + k^2 u_1 = 0 & \text{in } D, \\ u_1 = 0 & \text{on } \partial D, \\ \lim_{r\to\infty} \sqrt{r} \left(\dfrac{\partial u_1}{\partial r} - iku_1 \right) = 0 \end{cases} \tag{7}$$

and the interior problem

$$\begin{cases} \Delta u_2 + k^2 u_2 = 0 & \text{in } \tilde{D}, \\ u_2 = 0 & \text{on } \overline{\Gamma \cup \Gamma_r}. \end{cases} \tag{8}$$

If k^2 is not the eigenvalue of $-\Delta$ in $\tilde{D}$ for the Dirichlet problem, then (7) and (8) attains a unique solution respectively. Hence $\dfrac{\partial u_1}{\partial v} - \dfrac{\partial u_2}{\partial v} = 0$. By the limit of the single layer potential in Lemma 2.1 we have $-\psi = \dfrac{\partial u_1}{\partial v} - \dfrac{\partial u_2}{\partial v} = 0$ on Γ. Note that $\psi \in C(\overline{\Gamma})$, thus $\psi \equiv 0$ on $\overline{\Gamma}$.

2.2. SCATTERED WAVE IN THE NEAR-FIELD REGIME. Now we are ready to examine the scattered field in the near-field regime. It is shown that the exponentially decayed (evanescent) wave modes which are localized to the surface the local disturbance are significant in the near field. Furthermore, the connection between the evanescent wave modes and the high frequency components for the profile of the local disturbance is formulated explicitly .

For convenience, the Green's function $G(x, y)$ and the fundamental solution $\Phi(x, y)$ are written with an explicit dependence on the first variable:

$$G(x, y) = \tilde{G}(x_1 - y_1; x_2, y_2) := \tilde{\Phi}(x_1 - y_1, x_2 - y_2) - \tilde{\Phi}(x_1 - y_1, x_2 + y_2) \ ,$$

where $\tilde{\Phi}(x_1, x_2) = \dfrac{i}{4} H_0^{(1)}(k\sqrt{x_1^2 + x_2^2})$.

For the free space fundamental solution $\tilde{\Phi}(x_1 - y_1, x_2 - y_2)$, we have the following plane wave (Weyl) decomposition (Appendix B):

$$\tilde{\Phi}(x_1 - y_1, x_2 - y_2) = \frac{i}{4\pi} \int_{\mathbb{R}} \frac{1}{k_2(\kappa)} e^{i(x_1 - y_1)\cdot\kappa} e^{ik_2(\kappa)|x_2 - y_2|} d\kappa, \tag{9}$$

where

$$k_2(\kappa) = \begin{cases} \sqrt{k^2 - |\kappa|^2} & |\kappa| < k \quad \text{(propagating modes)}, \\ i\sqrt{|\kappa|^2 - k^2} & |\kappa| > k \quad \text{(evanescent modes)}. \end{cases} \tag{10}$$

The decomposition may be viewed as the sum of the plane waves that consist of propagating and evanescent modes. It is clear that all the wave modes propagate along the x_1 direction. Along the x_2 direction, when the magnitude of the spatial frequency $|\kappa|$ is below k, the wave mode also propagates; otherwise, it decays exponentially along the x_2 direction and is denoted as the evanescent mode.

A similar plane wave decomposition holds for $\tilde{G}(x_1 - y_1; x_2, y_2)$ evaluated at $x_2 = d$:

$$\tilde{G}(x_1 - y_1; d, y_2) = \frac{i}{4\pi} \int_{\mathbb{R}} \frac{1}{k_2(\kappa)} e^{i(x_1 - y_1)\cdot\kappa} \left(e^{ik_2(\kappa)|d - y_2|} - e^{ik_2(\kappa)|d + y_2|} \right) d\kappa. \tag{11}$$

Thus for the scattered field at $x = (x_1, d)$, by noting the single layer potential (1), some simple calculations yield

$$u(x_1, d) = \frac{i}{4\pi} \int_{\mathbb{R}} \int_{\overline{\gamma}} \frac{1}{k_2(\kappa)} e^{i(x_1 - y_1)\cdot\kappa} \left(e^{ik_2(\kappa)|d - f(y_1)|} - e^{ik_2(\kappa)|d + f(y_1)|} \right) \psi(y_1, f(y_1))\ J\ dy_1 d\kappa,$$

where $J = \sqrt{1 + |f'|^2}$. This implies that the measured scattered field u on the line $x_2 = d$ can also be viewed as the superposition of the propagating and evanescent wave modes. It is important to note that the evanescent modes with spatial

frequency beyond the wavenumber k decay exponentially along the x_2 direction, and are localized to the surface of the obstacle within one wavelength. Therefore, in the far-field regime, such evanescent modes carried by the scattered field are lost. However, in the near-field regime, the evanescent modes are significant, and the measured scattered field carries more information for the profile of the local disturbance to be reconstructed.

On the other hand, following from the Taylor expansion of $\tilde{G}(x_1 - y_1; d, y_2)$ at $y_2 = 0$, the scattered field can also be expanded as

$$\begin{aligned} u(x_1, d) &= \int_{\overline{\gamma}} [\tilde{G}(x_1 - y_1; d, 0) + \frac{\partial \tilde{G}(x_1 - y_1; d, 0)}{\partial y_2} f(y_1) + \frac{\partial^2 \tilde{G}(x_1 - y_1; d, 0)}{\partial y_2^2} (f(y_1))^2 \\ &\quad + O(f^3)]\, \psi(y_1, f(y_1))\, J\, dy_1 \,. \end{aligned}$$

where

(a) $\tilde{G}(x_1 - y_1; d, 0) = \dfrac{\partial^2 \tilde{G}(x_1 - y_1; d, 0)}{\partial y_2^2} = 0$ by the symmetry property of $\tilde{G}$;

(b) for the high order term, by a direct calculation, asymptotically

$$O(f^3) = O\left((\frac{f}{\lambda})^2\right) \frac{\partial G(x_1 - y_1; d, 0)}{\partial y_2} f.$$

We assume that $\left(\dfrac{f}{\lambda}\right)^2 \ll 1$, and denote $\varphi = \psi\sqrt{1 + |f'|^2}$. Then the scattered field is simplified as

$$\begin{aligned} u(x_1, d) &\approx \int_{\overline{\gamma}} \frac{\partial \tilde{G}(x_1 - y_1; d, 0)}{\partial y_2} f(y_1)\varphi(y_1) dy_1 \\ &= \int_{\mathbb{R}} \frac{\partial \tilde{G}(x_1 - y_1; d, 0)}{\partial y_2} f(y_1)\varphi(y_1) dy_1. \end{aligned} \tag{12}$$

The equality holds since the surface displacement is supported on γ. Here we implicitly extend the definition of f and φ to $\mathbb{R}$ by setting f as 0 for $x_1 \in \mathbb{R} \setminus \overline{\gamma}$. On the other hand, from (11) a simple calculation yields

$$\frac{\partial \tilde{G}(x_1 - y_1; d, 0)}{\partial y_2} = \frac{1}{2\pi} \int_{\mathbb{R}} e^{i(x_1 - y_1)\cdot\kappa} e^{ik_2(\kappa)d}\, d\kappa.$$

Therefore, by taking the Fourier transform of (12), we arrive at

$$\hat{u}(\kappa, d) \approx e^{ik_2(\kappa)d} \widehat{(f\varphi)}(\kappa), \quad \kappa \in \mathbb{R}\,, \tag{13}$$

where $\widehat{\cdot}$ denotes the Fourier transform.

Remark 1. The expression (13) formulates explicitly the connection between the evanescent wave modes and the high frequency components of the profile f. It indicates that a high spatial frequency mode of the scattered field $\hat{u}(\kappa, d)$ carries high spatial frequency information (fine features) of f to be reconstructed.

Remark 2. If $\frac{f}{\lambda} \ll 1$ and the modulus of its derivative $|f'| \ll 1$, then (13) is reduced automatically to the linear model discussed in [9].

Now we distinguish the far-field and the near-field cases based on (13). When the spatial frequency $|\kappa| > k$, $e^{ik_2(\kappa)d}$ decreases exponentially with respect to the distance d and its value vanishes when d exceeds one wavelength (see Figure 2). Thus in the far-field regime ($d \gg \lambda$), $\hat{u}(\kappa, d) \approx 0$ for $|\kappa| > k$, i.e., the high spatial

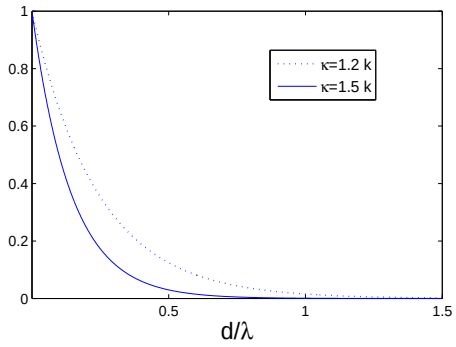

FIGURE 2. $e^{ik_2(\kappa)d}$ for $d \in (0, 1.5\lambda)$ when the spatial frequency $\kappa = 1.2k$ and $1.5k$ respectively .

frequency information of f is lost in the far-field measurement. In the context of imaging, this implies that it is impossible to recover f with very high resolution when any noise is present. However, in the near-field regime with $d < \lambda$, $e^{ik_2(\kappa)d}$ is not close to 0 and the exponentially decayed modes are still significant in the scattered field. Therefore, the higher spatial frequency components of f can still be retrieved by inverting the evanescent modes of the scattered field.

3. Near-field imaging

3.1. Inversion method. Assume that the measurement $u(\cdot, d)$ is polluted with some additive noise $n(x_1)$, which takes the following form

$$n(x_1) = \sigma \cdot \text{rand}(x_1) \cdot u(x_1, d).$$

σ is the noise level, and $\text{rand}(x_1)$ is a uniformly distributed random variable in $[-1, 1]$ for each $x_1 \in \mathbb{R}$. Moreover, $\text{rand}(x_1)$ is mutually independent for different values of x_1.

Based on the previous analysis, we present a reconstruction method. From (13), we introduce the pseudo-inverse operator $\mathbf{I}_d$ as follows:

$$\mathbf{I}_d(\kappa) = \begin{cases} e^{-ik_2(\kappa)d} & |\kappa| \le k_c, \\ 0 & |\kappa| > k_c \ , \end{cases} \tag{1}$$

where $\mathbf{I}_d(\kappa)$ is a cut-off regularized operator, and k_c is a regularization parameter. For other regularization techniques such as the classical Tikhonov regularization and the Landweber iteration, we refer the reader to [7, 10, 12, 14, 19] for detailed discussions.

In the far-field case, as we discuss in the previous section, only the propagating modes can be used for imaging if noise is present, thus the cutoff frequency $k_c = k$. In the near-field regime, the bandwidth of the spatial frequency is expanded beyond the wavenumber k by taking account of the evanescent waves. Note that $e^{-ik_2(\kappa)d}$ is an exponentially increasing function with respect to $|\kappa|$ when $|\kappa| > k$. Hence, the noise may be exponentially amplified for large $|\kappa|$. For fixed distance d, the cutoff frequency k_c depends on the noise level (or signal-to-noise ratio). Here, following [9], we choose k_c in such a way that

$$e^{ik_2(k_c)d} = e^{-\sqrt{k_c^2 - k^2}\, d} = \sigma. \tag{2}$$

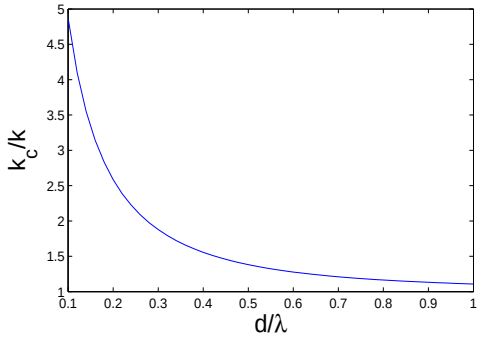

FIGURE 3. k_c/k versus the distance varying from $\lambda/10$ to λ.

That is, the spatial frequency with the transfer function $e^{ik_2(\kappa)d}$ below the noise level σ is cut off. More explicitly,

$$k_c = \left(k^2 + \left(\frac{\log \frac{1}{\sigma}}{d} \right)^2 \right)^{1/2}. \tag{3}$$

In view of (2) or (3), the pseudo-inverse (1) offers a regularization strategy for the inverse problem. We plot the function k_c/k for various distance d in Figure 3 at 5% noise level. It is easily seen that at the fixed noise level, the cutoff frequency $k_c \gg k$ when $d < \lambda$, i.e., the bandwidth of the spatial frequency in the near field is much larger than in the far field. This guarantees better resolution for the final reconstruction in the near-field regime, since the higher spatial frequency components of f are recovered.

Denote

$$\hat{h}(\kappa) = \mathbf{I}_d(\kappa)\hat{u}(\kappa, d). \tag{4}$$

To compute h, the FFT may be applied to compute the inverse Fourier transform, where h is an approximation of $f\varphi$. To reconstruct f from h, we need to take into account of the boundary data on Γ, which turns out to be a (well-posed) nonlinear problem.

We next introduce some notations for representing the surface displacement f.

Denote by $C^{0,1}(\overline{\gamma})$ the set of Lipschitz continuous functions on $\overline{\gamma}$. Introduce the Banach space $C_0^{0,1}(\overline{\gamma}) := \{f \mid f \in C^{0,1}(\overline{\gamma}), f = 0 \text{ on } \partial\gamma\}$ with the usual norm

$$\|f\|_{0,1} = \|f\|_\infty + sup_{x_1, y_1 \in \gamma, x_1 \neq y_1} \frac{|f(x_1) - f(y_1)|}{|x_1 - y_1|}.$$

For a fixed small number δ, we define

$$\gamma_\delta := \{x_1 \in \gamma \mid dist(x_1, \partial\gamma) < \delta\}.$$

For $x_1 \in \gamma_\delta$, let $x_b \in \partial\gamma$ such that $|x_1 - x_b| = dist(x_1, \partial\gamma)$. Assume that $\{ x_1^0, x_1^1, x_1^2 \cdots x_1^N \}$ is a set of grid points defined on $\overline{\gamma}$. We represent f by a piecewise linear function, where

f is linear on $[x_1^{j-1}, x_1^j]$ for $j = 1, 2, \cdots, N$, and is continuous on $\overline{\gamma}$ globally.

Moreover, f is strictly greater than 0 for the interior grid points x_1^1, $x_1^2 \cdots x_1^{N-1}$, and is 0 on the boundary x_1^0, x_1^N. We denote the set of all such functions by $\mathcal{P}_1$. It is clear that $\mathcal{P}_1$ is a subset of $\tilde{C}_0^{0,1}(\overline{\gamma})$, which is defined as follows:

$$\tilde{C}_0^{0,1}(\overline{\gamma}) := \{f \in C_0^{0,1}(\overline{\gamma}) \mid f(x_1) > 0 \text{ for } x_1 \in \gamma;\ \exists\, \epsilon, \delta > 0,\ s.t.\ f(x_1) \geq \epsilon\,|x_1 - x_b| \text{ for } x_1 \in \gamma_\delta\}.$$

For fixed grid points $\{ x_1^0, x_1^1, x_1^2 \cdots x_1^N \}$, $\delta = \min\{\left|x_1^1 - x_1^0\right|, \left|x_1^N - x_1^{N-1}\right|\}$, $\epsilon = \min\{\frac{f(x_1^1)}{\left|x_1^1 - x_1^0\right|}, \frac{f(x_1^{N-1})}{\left|x_1^N - x_1^{N-1}\right|}\}$. On the other hand, $\tilde{C}_0^{0,1}(\overline{\gamma})$ is an open subset of $C_0^{0,1}(\overline{\gamma})$.

We rewrite the integral operator (6) on $\overline{\gamma}$ by introducing the operator $\tilde{K}_f$ defined as

$$(\tilde{K}_f\varphi)(x_1) := \int_{\overline{\gamma}} G(x_1 - y_1; f(x_1), f(y_1))\varphi(y_1)dy_1, \quad x_1 \in \overline{\gamma}, \tag{5}$$

where $\varphi = \psi\sqrt{1 + |f'|^2}$. The kernel of the integral operator $\tilde{K}_f$ has explicit dependence on f. Here we adopt the subscript for $\tilde{K}_f$ to emphasize its dependence on f. Similarly, define $\tilde{g}_f(x_1) := g(x_1, f(x_1))$, where $g = -(u^i + u^r)|_{\overline{\Gamma}}$ is the boundary data.

A natural way of separating f from h computed in (4) is to minimize the functional

$$\min_{f \in \mathcal{P}_1} \left(\left\| \tilde{K}_f\varphi - \tilde{g}_f \right\|_{L^2(\gamma)} + \|f\varphi - h\|_{L^2(\gamma)} \right). \tag{6}$$

However, this minimization problem is difficult to solve in practice, since f and φ are both unknowns. One alternative is to solve

$$\min_{f \in \mathcal{P}_1} \|f\varphi - h\|_{L^2(\gamma)} \quad \text{subject to } \tilde{K}_f\varphi = \tilde{g}_f.$$

It should be pointed out that in general φ is not Fréchet differentiable with respect to f since the operator $\tilde{K}_f$ is compact. Therefore, existing numerical methods such as Newton's method can not be applied directly.

We introduce a new function h_0 such that h_0 is Lipschitz continuous on $\bar{\gamma}$, moreover

$$h_0(x_1) = \begin{cases} h(x_1) & x_1 \in \gamma\backslash\gamma_\delta, \text{ for sufficiently small } \delta; \\ 0 & x_1 \in \partial\gamma. \end{cases} \tag{7}$$

By choosing a small δ (usually the length of two neighboring grid points), $\|h_0 - h\|_{L^2(\gamma)}$ is small. In practice, h_0 may be chosen as the following piecewise linear function:

$$h_0(x_1^j) = \begin{cases} h(x_1^j) & j = 1, 2, \cdots, N-1; \\ 0 & j = 0, N. \end{cases}$$

Now we match the data on the boundary by solving the minimization problem with a constraint:

$$\min_{f \in \mathcal{P}_1} \left\| \tilde{K}_f\varphi - \tilde{g}_f \right\|_{L^2(\gamma)} \quad \text{where } \varphi \in C(\overline{\gamma}) \text{ satisfies } f\varphi = h_0. \tag{8}$$

Remark 3. The minimization problem (8) is a special case of (6). By letting $f\varphi = h_0$, (6) becomes

$$\min \left\| \tilde{K}_f\varphi - \tilde{g}_f \right\|_{L^2(\gamma)} + \|h_0 - h\|_{L^2(\gamma)},$$

and $\|h_0 - h\|_{L^2(\gamma)}$ is small by the definition of h_0.

Remark 4. For $f \in \mathcal{P}_1 \subset \tilde{C}_0^{0,1}(\overline{\gamma})$, the function $\varphi \in C(\overline{\gamma})$ that satisfies $f\varphi = h_0$ is well defined. Moreover

$$\|\varphi\|_\infty \leq (\frac{1}{\min_{x_1 \in \gamma \setminus \gamma_\delta} f(x_1)} + 1/\epsilon) \|h_0\|_{0,1} .$$

The problem (8) can be solved by Newton's method. Since $(\frac{f}{\lambda})^2 \ll 1$, the iteration is expected to converge fast to the real solution, which is confirmed by our numerical examples. To linearize the problem, we require the mapping $F(f) := \tilde{K}_f\varphi - \tilde{g}_f$ be Fréchet differentiable with respect to $f \in \mathcal{P}_1$.

3.2. DIFFERENTIABILITY OF THE MAPPING $F(f) := \tilde{K}_f\varphi - \tilde{g}_f$. Here and thereafter, M and $\tilde{M}$ stand for some generic positive constants, whose values may vary from step to step but should be clear from the contexts. Let $\mathcal{L}(C(\overline{\gamma}), C(\overline{\gamma}))$ be the set of all bounded linear operators that map the functional space $C(\overline{\gamma})$ to itself.

Lemma 3.1. *If $f \in \tilde{C}_0^{0,1}(\overline{\gamma}) \subset C_0^{0,1}(\overline{\gamma})$, then the mapping $f \to \tilde{K}_f$ is Fréchet differentiable from $C_0^{0,1}(\overline{\gamma})$ to $\mathcal{L}(C(\overline{\gamma}), C(\overline{\gamma}))$. Moreover, the Fréchet derivative is the linear mapping $\delta_f \to (\tilde{K}_f)'(\delta_f)$ for $\delta_f \in C_0^{0,1}(\overline{\gamma})$, where $(\tilde{K}_f)'(\delta_f) \in \mathcal{L}(C(\overline{\gamma}), C(\overline{\gamma}))$ is defined as*

$$\begin{aligned}[(\tilde{K}_f)'(\delta_f)]\varphi(x_1) &= \int_{\overline{\gamma}} \big[\frac{\partial\tilde{\Phi}(x_1 - y_1, f(x_1) - f(y_1))}{\partial x_2}(\delta_f(x_1) - \delta_f(y_1)) \\ &\quad - \frac{\partial\tilde{\Phi}(x_1 - y_1, f(x_1) + f(y_1))}{\partial x_2}(\delta_f(x_1) + \delta_f(y_1))\big]\varphi(y_1)dy_1\end{aligned}$$

for $\varphi \in C(\overline{\gamma})$.

Proof. It is clear that the mapping $\delta_f \to (\tilde{K}_f)'(\delta_f)$ is linear.

Step1: the mapping $\delta_f \to (\tilde{K}_f)'(\delta_f)$ is bounded.

Denote

$$r_1 = \sqrt{(x_1 - y_1)^2 + (f(x_1) - f(y_1))^2},\ \ r_2 = \sqrt{(x_1 - y_1)^2 + (f(x_1) + f(y_1))^2}.$$

We first estimate the first part:

$$\left|\frac{\partial\tilde{\Phi}(x_1 - y_1, f(x_1) - f(y_1))}{\partial x_2}\right| = \left|\frac{ik}{4}\left(H_0^{(1)}(kr_1)\right)' \frac{f(x_1) - f(y_1)}{r_1}\right| \leq \frac{k}{4}\left|\left(H_0^{(1)}(kr_1)\right)'\right|.$$

For a small fixed constant τ_0, if $|y_1 - x_1| \geq \tau_0$ (away from the singularity), then

$$\left|\left(H_0^{(1)}(kr_1)\right)'\right| \leq \tilde{M} .$$

It follows that

$$\left|\int_{\overline{\gamma}\setminus\{|y_1 - x_1| < \tau_0\}} \frac{\partial\tilde{\Phi}(x_1 - y_1, f(x_1) - f(y_1))}{\partial x_2}(\delta_f(x_1) - \delta_f(y_1))\varphi(y_1)dy_1\right| \leq M \|\delta_f\|_{0,1} \|\varphi\|_\infty .$$

On the other hand, if $|y_1 - x_1| < \tau_0$, $\left|\left(H_0^{(1)}(kr_1)\right)'\right| \sim O(\frac{1}{r_1})$ for τ_0 sufficiently small. We have

$$\begin{aligned} & \left| \int_{\{|y_1-x_1|<\tau_0\}} \frac{\partial \tilde{\Phi}(x_1-y_1, f(x_1)-f(y_1))}{\partial x_2} (\delta_f(x_1)-\delta_f(y_1))\varphi(y_1) dy_1 \right| \\ \leq & \int_{\{|y_1-x_1|<\tau_0\}} \frac{M}{r_1} |x_1-y_1| \, dy_1 \, \|\delta_f\|_{0,1} \, \|\varphi\|_\infty \leq M \, \|\delta_f\|_{0,1} \, \|\varphi\|_\infty . \end{aligned}$$

For the second part,

$$\begin{aligned} & \int_{\overline{\gamma}} \frac{\partial \tilde{\Phi}(x_1-y_1, f(x_1)+f(y_1))}{\partial x_2} (\delta_f(x_1)+\delta_f(y_1))\varphi(y_1) dy_1 \\ = & \int_{\overline{\gamma}} \frac{\partial \tilde{\Phi}(x_1-y_1, f(x_1)+f(y_1))}{\partial x_2} [\delta_f(y_1)-\delta_f(x_1)]\varphi(y_1) dy_1 \\ + & 2\int_{\overline{\gamma}} \frac{\partial \tilde{\Phi}(x_1-y_1, f(x_1)+f(y_1))}{\partial x_2} \varphi(y_1) dy_1 \delta_f(x_1) \\ =: & \mathcal{A}_1 + \mathcal{A}_2 \end{aligned}$$

From the estimate of the first term, the following inequality also holds:

$$|\mathcal{A}_1| \leq M \, \|\delta_f\|_{0,1} \, \|\varphi\|_\infty .$$

For $x_1 \in \gamma \backslash \gamma_{\frac{\delta}{2}}$,

$$|\mathcal{A}_2| \leq M_\delta \, \|\delta_f\|_{0,1} \, \|\varphi\|_\infty , \quad \text{where } M_\delta = \frac{k}{2} \min_{x_1 \in \gamma \backslash \gamma_{\frac{\delta}{2}}} \left| \left(H_0^{(1)}(kf(x_1))\right)' \right| .$$

For $x_1 \in \gamma_{\frac{\delta}{2}}$,

$$\begin{aligned} |\mathcal{A}_2| & \leq \frac{k}{2} \left(\int_{\overline{\gamma} \backslash [x_1-\delta/2, x_1+\delta/2]} + \int_{[x_1-\delta/2, x_1+\delta/2]} \right) \left| \left(H_0^{(1)}(kr_2)\right)' \right| \, dy_1 \, |\delta_f(x_1)| \, \|\varphi\|_\infty \\ & \leq \tilde{M} \left| \left(H_0^{(1)}(\frac{k\delta}{2}) \right)' \right| \|\delta_f\|_{0,1} \, \|\varphi\|_\infty + \tilde{M} \int_{x_1-\delta/2}^{x_1+\delta/2} \frac{1}{\sqrt{(y_1-x_1)^2 + f(x_1)^2}} dy_1 \, |\delta_f(x_1)| \, \|\varphi\|_\infty \\ & \leq \tilde{M} \left[\left| \left(H_0^{(1)}(\frac{k\delta}{2}) \right)' \right| + \ln 2 - \ln(1 - \frac{\delta}{\sqrt{\delta^2 + (\epsilon/2)^2 \, |x_1-x_b|^2}}) \, |x_1-x_b| \right] \|\delta_f\|_{0,1} \, \|\varphi\|_\infty . \end{aligned}$$

The last inequality follows from the fact that there exists an ϵ such that $f(x_1) \geq \epsilon \, |x_1 - x_b|$ for $x_1 \in \gamma_\delta$, and $|\delta_f(x_1)| \leq \|\delta_f\|_{0,1} \, |x_1 - x_b|$.

Therefore

$$|\mathcal{A}_2| \leq M(\epsilon, \delta) \, \|\delta_f\|_{0,1} \, \|\varphi\|_\infty \ ,$$

where

$$M(\epsilon, \delta) = \tilde{M} \left[\left| \left((H_0^{(1)}(\frac{k\delta}{2}) \right)' \right| + \ln 2 - \inf_{x_1 \in \gamma_{\delta/2}} \left(\ln(1 - \frac{\delta}{\sqrt{\delta^2 + (\epsilon/2)^2 \, |x_1-x_b|^2}}) \, |x_1-x_b| \right) \right]$$

is a positive constant.

Therefore

$$\left\| [(\tilde{K}_f)'(\delta_f)]\varphi \right\|_\infty \leq M(\epsilon, \delta, f) \, \|\delta_f\|_{0,1} \, \|\varphi\|_\infty$$

for any $\varphi \in C(\overline{\gamma})$, i.e.,

$$\left\|(\tilde{K}_f)'(\delta_f)\right\|_{\mathcal{L}(C(\overline{\gamma}),C(\overline{\gamma}))} \leq M(\epsilon,\delta,f)\left\|\delta_f\right\|_{0,1}.$$

Step2: An estimate of the remainder term $\tilde{K}_{f+\delta f} - \tilde{K}_f - (\tilde{K}_f)'(\delta_f)$.

For any $\varphi \in C(\overline{\gamma})$, by Taylor's formula,

$$\begin{aligned}
&[\tilde{K}_{f+\delta f} - \tilde{K}_f - (\tilde{K}_f)'(\delta_f)]\varphi(x_1)\\
=\ & \int_{\overline{\gamma}}\int_0^1 \frac{\partial^2\tilde{\Phi}(x_1-y_1, f(x_1)-f(y_1)+t(\delta_f(x_1)-\delta_f(y_1))\,)}{\partial x_2^2} dt[\delta_f(x_1)-\delta_f(y_1)]^2\varphi(y_1)dy_1\\
-\ & \int_{\overline{\gamma}}\int_0^1 \frac{\partial^2\tilde{\Phi}(x_1-y_1, f(x_1)+f(y_1)+t(\delta_f(x_1)+\delta_f(y_1))\,)}{\partial x_2^2} dt[\delta_f(x_1)+\delta_f(y_1)]^2\varphi(y_1)dy_1\\
=\ & \mathcal{B}_1+\mathcal{B}_2.
\end{aligned}$$

By a similar argument as in Step 1, we can estimate $\mathcal{B}_1$. Assume that $\|\delta_f\|_{0,1}$ is sufficiently small. For a fixed small constant τ_0, if $|y_1-x_1| \geq \tau_0$ (away from singularity), then

$$\begin{aligned}
&\left|\int_{\overline{\gamma}\setminus\{|y_1-x_1|<\tau_0\}}\int_0^1 \frac{\partial^2\tilde{\Phi}(x_1-y_1, f(x_1)-f(y_1)+t(\delta_f(x_1)-\delta_f(y_1))\,)}{\partial x_2^2} dt[\delta_f(x_1)-\delta_f(y_1)]^2\varphi(y_1)dy_1\right|\\
&\leq M\left\|\delta_f\right\|_{0,1}^2\left\|\varphi\right\|_\infty.
\end{aligned}$$

If $|y_1-x_1|<\tau_0$, $\left|\dfrac{\partial^2\tilde{\Phi}}{\partial x_2^2}\right| \sim O(\dfrac{1}{r_1^2})$ for τ_0 sufficiently small. Thus

$$\begin{aligned}
&\left|\int_{\{|y_1-x_1|<\tau_0\}}\int_0^1 \frac{\partial^2\tilde{\Phi}(x_1-y_1, f(x_1)-f(y_1)+t(\delta_f(x_1)-\delta_f(y_1))\,)}{\partial x_2^2} dt[\delta_f(x_1)-\delta_f(y_1)]^2\varphi(y_1)dy_1\right|\\
&\leq \int_{\{|y_1-x_1|<\tau_0\}} \frac{M}{r_1^2}\left|x_1-y_1\right|^2 dy_1\left\|\delta_f\right\|_{0,1}^2\left\|\varphi\right\|_\infty \leq M\left\|\delta_f\right\|_{0,1}^2\left\|\varphi\right\|_\infty.
\end{aligned}$$

Next, the term $\mathcal{B}_2$ can also be split into two parts $\mathcal{B}_2^1$ and $\mathcal{B}_2^2$:

$$\mathcal{B}_2^1 = \int_{\overline{\gamma}}\int_0^1 \frac{\partial^2\tilde{\Phi}(x_1-y_1, f(x_1)+f(y_1)+t(\delta_f(x_1)+\delta_f(y_1))\,)}{\partial x_2^2} dt[\delta_f(x_1)-\delta_f(y_1)]^2\varphi(y_1)dy_1$$

and

$$\mathcal{B}_2^2 = 4\int_{\overline{\gamma}}\int_0^1 \frac{\partial^2\tilde{\Phi}(x_1-y_1, f(x_1)+f(y_1)+t(\delta_f(x_1)+\delta_f(y_1))\,)}{\partial x_2^2} dt[\delta_f(x_1)\delta_f(y_1)]\varphi(y_1)dy_1.$$

It suffices to estimate $\mathcal{B}_2^2$. For $x_1 \in \gamma\setminus\gamma_{\frac{\delta}{2}}$,

$$\left|\mathcal{B}_2^2\right| \leq M_\delta\left\|\delta_f\right\|_{0,1}^2\left\|\varphi\right\|_\infty, \quad \text{where } M_\delta = \min_{x_1\in\gamma\setminus\gamma_{\frac{\delta}{2}}} k^2\left|\left(H_0^{(1)}(\frac{2k}{f(x_1)})\right)''\right| + \frac{2k}{f(x_1)}\left|\left(H_0^{(1)}(\frac{2k}{f(x_1)})\right)'\right|$$

if $\|\delta_f\|_{0,1}$ is sufficiently small.

For $x_1 \in \gamma_{\frac{\delta}{2}}$,

$$\begin{aligned}
\left|\mathcal{B}_2^2\right| &\leq \left(\int_{\overline{\gamma}\setminus[x_1-\delta/2,x_1+\delta/2]} + \int_{[x_1-\delta/2,x_1+\delta/2]}\right)\left(\int_0^1 \left|\frac{\partial^2\tilde{\Phi}}{\partial x_2^2}\right| dt\right) dy_1 \left|\delta_f(x_1)\right| \left\|\delta_f\right\|_{0,1} \left\|\varphi\right\|_\infty \\
&\leq \tilde{M}_\delta \left\|\delta_f\right\|_{0,1}^2 \left\|\varphi\right\|_\infty + \tilde{M}\int_{x_1-\delta/2}^{x_1+\delta/2} \frac{1}{(y_1-x_1)^2+(\epsilon/2)^2\left|x_1-x_b\right|^2} dy_1 \left|\delta_f(x_1)\right| \left\|\delta_f\right\|_{0,1} \left\|\varphi\right\|_\infty \\
&\leq \tilde{M}_\delta \left\|\delta_f\right\|_{0,1}^2 \left\|\varphi\right\|_\infty + \frac{\tilde{M}}{\epsilon/2\left|x_1-x_b\right|} \left|\delta_f(x_1)\right| \left\|\delta_f\right\|_{0,1} \left\|\varphi\right\|_\infty . \\
&\leq M(\epsilon,\delta) \left\|\delta_f\right\|_{0,1}^2 \left\|\varphi\right\|_\infty .
\end{aligned}$$

Therefore

$$\left\|\tilde{K}_{f+\delta f} - \tilde{K}_f - (\tilde{K}_f)'(\delta_f)\right\|_{\mathcal{L}(C(\overline{\gamma}),C(\overline{\gamma}))} = O(\|\delta_f\|_{0,1}^2) ,$$

for sufficiently small $\left\|\delta_f\right\|_{0,1}$, which completes the proof.

□

Let $h_0 \in C_0^{0,1}(\overline{\gamma})$ be defined as in (7). For $f \in \mathcal{P}_1 \subset \tilde{C}_0^{0,1}(\overline{\gamma})$, let $\varphi \in C(\overline{\gamma})$ satisfy $f\varphi = h_0$. The following lemma concerns the Fréchet derivative of the mapping $f \to \varphi$ ($C_0^{0,1}(\overline{\gamma}) \to C(\overline{\gamma})$).

Lemma 3.2. *If $f \in \tilde{C}_0^{0,1}(\overline{\gamma}) \subset C_0^{0,1}(\overline{\gamma})$, then the mapping $f \to \varphi$ defined as the above is Fréchet differentiable from $C_0^{0,1}(\overline{\gamma})$ to $C(\overline{\gamma})$. Moreover, its Fréchet derivative is the linear mapping $\delta_f \to \varphi'$ for $\delta_f \in C_0^{0,1}(\overline{\gamma})$, where $\varphi' \in C(\overline{\gamma})$ and*

$$\varphi'(x_1) = -\frac{\varphi(x_1)}{f(x_1)}\delta f(x_1) \text{ for } x_1 \in \gamma.$$

Proof. It is easy to show that

$$|\varphi'(x_1)| \leq (M_\delta + \frac{1}{\epsilon}) \left\|\varphi\right\|_\infty \left\|\delta_f\right\|_{0,1} \quad \text{for } x_1 \in \gamma ,$$

where $M_\delta = \min_{x_1\in\gamma\setminus\gamma_\delta} \dfrac{1}{f(x_1)}$ is a constant. Therefore

$$\left\|\varphi'\right\|_\infty \leq (M_\delta + \frac{1}{\epsilon}) \left\|\varphi\right\|_\infty \left\|\delta_f\right\|_{0,1}$$

and the mapping $\delta_f \to \varphi'$ is bounded from $C_0^{0,1}(\overline{\gamma}) \to C(\overline{\gamma})$.

For a perturbation of f with $\delta_f \in C_0^{0,1}(\overline{\gamma})$, a perturbation of φ satisfies

$$(\varphi + \delta_\varphi)(f + \delta_f) = h_0.$$

If $\left\|\delta_f\right\|_{0,1}$ is sufficiently small, for $x_1 \in \gamma$, the following estimate for the high order term holds:

$$|(\varphi+\delta_\varphi)(x_1) - \varphi(x_1) - \varphi'(x_1)| = \left|\frac{1}{(f(x_1)+\delta_f(x_1))f(x_1)}\right| |\varphi(x_1)|\,|\delta_f(x_1)| \leq \frac{1}{2}(M_\delta^2+\frac{1}{\epsilon^2}) \left\|\varphi\right\|_\infty \left\|\delta_f\right\|_{0,1}^2 .$$

Thus

$$\left\|(\varphi+\delta_\varphi) - \varphi - \varphi'\right\|_\infty = O(\|\delta_f\|_{0,1}^2),$$

for sufficiently small $\left\|\delta_f\right\|_{0,1}$.

□

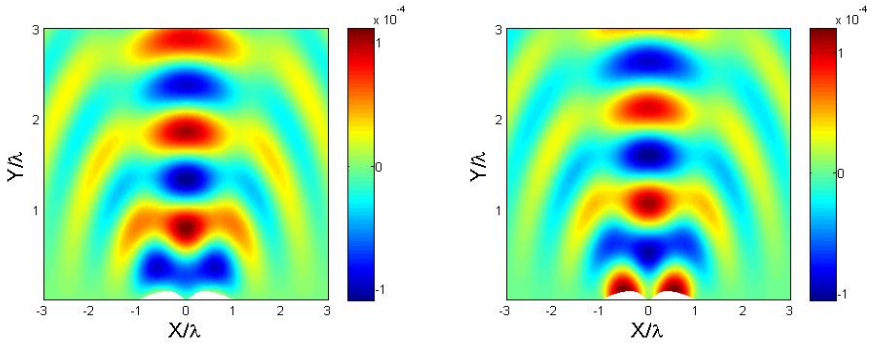

FIGURE 4. Real part (left) and the imaginary part (right) of the scattered field.

By Taylor's expansion, it is easily seen that the mapping $f \to \tilde{g}_f (:= g(x_1, f(x_1)))$ is also Fréchet differentiable from $C_0^{0,1}(\overline{\gamma})$ to $C(\overline{\gamma})$. We denote its Fréchet derivative as the mapping $\delta_f \to \tilde{g}'_f$. Combining Lemma 3.1 and Lemma 3.2 and using the product rule, we have the following theorem:

Theorem 3.3. *If $f \in \tilde{C}_0^{0,1}(\overline{\gamma}) \subset C_0^{0,1}(\overline{\gamma})$, $F(f) := \tilde{K}_f\varphi - \tilde{g}_f$ is Fréchet differentiable from $C_0^{0,1}(\overline{\gamma})$ to $C(\overline{\gamma})$. Moreover, the Fréchet derivative maps δ_f to $DF(\delta f) = [(\tilde{K})'_f(\delta_f)]\varphi + \tilde{K}_f(\varphi') - \tilde{g}'_f$.*

4. NUMERICAL EXAMPLES

First, let us consider the solution of the forward scattering problem. By Proposition 1, if k^2 is not an eigenvalue of $-\Delta$ in $\tilde{D}$, to solve the forward scattering problem (1)-(3) efficiently in our numerical simulation, we can firstly solve the integral equation $K\psi = g$ and substitute ψ into (1). If k^2 is an eigenvalue, then the forward scattering problem can be solved by introducing the artificial boundary (e.g. half circle) and solving the problem in a bounded domain. Since our focus is on inverse problem, without loss of generality, we assume that k^2 is not an eigenvalue in our numerical examples.

In the following examples, an incident wave $u^i = e^{ikq\cdot x}/100^2$ with normal incident direction impinges on the obstacle. The wavenumber $k = 100$, $\lambda \approx 6.28$ cm, $q = (0, -1)^T$. In all the figures, the plots are rescaled with respect to the wavelength λ.

Example 4.1. The real surface displacement is represented by two bumps, each one with the size of order λ. The two bumps are close to each other, and separated with distance $\lambda/10$. The scattered field in the region $[-3\lambda, 3\lambda]\times[0, 3\lambda]$ is plotted in Figure 4. Data are collected above the obstacle with distance $d = \lambda/5$ (near-field). We also assume that 5% noise is added to the simulation data. It follows from (3) that $k_c \approx 2.6k$. The near-field image f_n and the real image f are plotted in Figure 5 (left). Though two bumps are close to each other ($\lambda/10$), they are clear distinguishable. Therefore, super-resolution is achieved with near-field measurements. To confirm the convergence of Newton's method for solving the minimization problem (8), the relative error is shown with respect to the iteration number in Figure 6. Here the

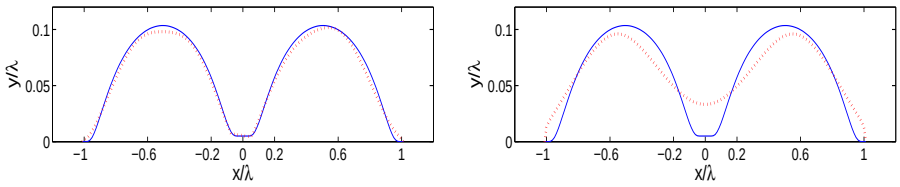

FIGURE 5. Near-field (left) and far-field (right) images. The solid line represents the real image, and the dotted line is the reconstruction.

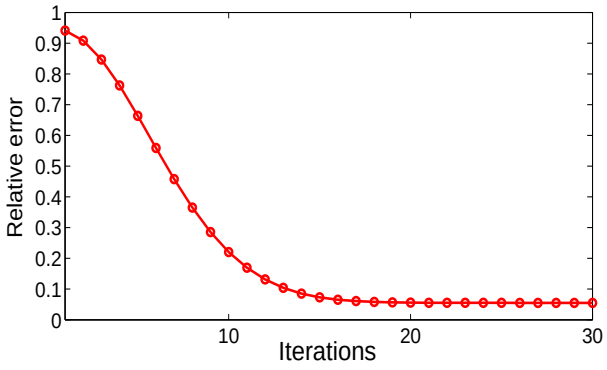

FIGURE 6. Relative error with respect to the Newton iterations.

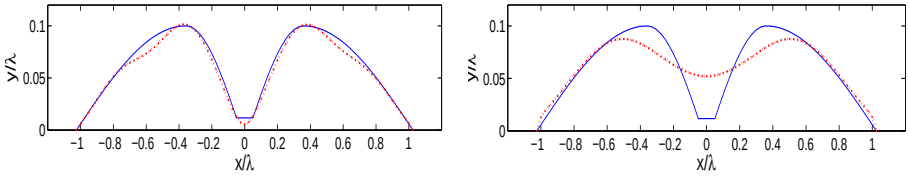

FIGURE 7. Near-field (left) and far-field (right) images. The solid line represents the real image, and the dotted line is the reconstruction.

relative error is defined as

$$\frac{\left(\sum_{j=0}^{N}\left|f(x_1^j)-f_n(x_1^j)\right|^2\right)^{1/2}}{\left(\sum_{j=0}^{N}f(x_1^j)^2\right)^{1/2}}.$$

The reconstruction converges fast, which leads to the real surface displacement after the first 20 iterations.

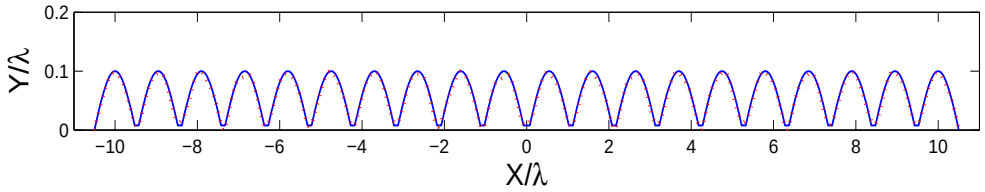

FIGURE 8. Comparison of the reconstruction (dotted line) with the real profile (solid line) for the near-field case.

To compare with the far-field image, we collect the data again with $d = 5\lambda$ and 5% noise. It is obvious that $k_c = k$ in the far-field case. The image f_n is shown in Figure 5 (right). It is clear that the two bumps can not be distinguished, which is due to the fact that the high spatial frequency information of the surface displacement is lost.

Example 4.2 We consider a non-smooth profile in this example. Two bumps are also separated with distance $\lambda/10$. The measurement is polluted with 5% noise. Figure 7 is the reconstructed near-field and far-field images when $d = \lambda/5$ and 5λ respectively. Super-resolution is still achieved via near-field imaging, and the accuracy of the reconstruction is deteriorated when data is collected at far field.

Example 4.3 The real surface displacement is a long periodic structure (see Figure 8, solid line). Each period is a bump with size of order λ, and two neighboring bumps are separated with distance $\lambda/10$. The measurement distance d again is $\lambda/5$, where 5% noise is added to the simulation data. We compare the near-field image and the real image in Figure 8. The periodic structure is also accurately reconstructed with super-resolution.

5. SUMMARY AND DISCUSSION

We study the near-field imaging of the local surface displacement on an infinite ground plane. An analysis of the scattered field is carried out, which indicates that in the far-field regime, the high spatial frequency information of the surface displacement is lost due to inaccessibility of the evanescent modes. However, in the near-field, the evanescent modes become significant, for which high spatial frequency modes of the surface displacement may be recovered. A numerical method is proposed in the near-field regime that yields super-resolution for the reconstructed image.

Numerically, the Newton iteration for the minimization problem (8) converges fast to the real solution. However, no rigorous theoretical convergence analysis is presently available. Another issue is denoising in the near-field regime. Noise will be exponentially amplified in near-field regime. The cutoff wavenumber k_c, which is the critical parameter for the resolution of the reconstructed image, strongly depends on the noise level. A denosing technique based on the broadband signal has recently been proposed in [9] for the linearized model. For the nonlinear imaging, the problem becomes much more challenging and is completely open.

ACKNOWLEDGMENTS

We thank Professor George C. Papanicolaou for directing our attention to their paper [9] which motivates our work. We also thank the referees for useful comments and suggestions.

APPENDIX A. PROOF OF LEMMA 2.1

For $x \in \Gamma$, $\epsilon > 0$, denote $\Gamma_{x,\epsilon} := \{\, y \in \Gamma,\ |y - x| < \epsilon \,\}$. We first show that

$$\lim_{\epsilon \to 0} \lim_{h \to 0^+} \int_{\Gamma_{x,\epsilon}} \frac{\partial \Phi(x + h\nu_x, y)}{\partial \nu_x} ds_y = -\frac{1}{2}.$$

Let $\partial\Omega$ (the boundary of some bounded connected domain Ω) be a C^2 closed curve such that $\Gamma \subset \partial\Omega$. Moreover, for $x \in \Gamma$, the unit outward normal of x on $\partial\Omega$ coincides with ν_x. Let $\psi \equiv 1$ on $\partial\Omega$, from the classical results in [6, 7],

$$\left(\frac{\partial u}{\partial \nu}\right)_+ (x) = \int_{\partial\Omega} \frac{\partial \Phi(x,y)}{\partial \nu_x} ds_y - \frac{1}{2}, \quad x \in \Gamma. \tag{9}$$

On the other hand, for any small fixed number $\epsilon > 0$,

$$\begin{aligned} \lim_{h \to 0^+} \int_{\partial\Omega} \frac{\partial \Phi(x + h\nu_x, y)}{\partial \nu_x} ds_y &= \lim_{h \to 0^+} \left[\int_{\partial\Omega \setminus \Gamma_{x,\epsilon}} + \int_{\Gamma_{x,\epsilon}} \right] \frac{\partial \Phi(x + h\nu_x, y)}{\partial \nu_x} ds_y \\ &= \int_{\partial\Omega \setminus \Gamma_{x,\epsilon}} \frac{\partial \Phi(x,y)}{\partial \nu_x} ds_y + \lim_{h \to 0^+} \int_{\Gamma_{x,\epsilon}} \frac{\partial \Phi(x,y)}{\partial \nu_x} ds_y. \end{aligned}$$

Now letting $\epsilon \to 0$, we get

$$\lim_{h \to 0^+} \int_{\partial\Omega} \frac{\partial \Phi(x + h\nu_x, y)}{\partial \nu_x} ds_y = \int_{\partial\Omega} \frac{\partial \Phi(x,y)}{\partial \nu_x} ds_y + \lim_{\epsilon \to 0} \lim_{h \to 0^+} \int_{\Gamma_{x,\epsilon}} \frac{\partial \Phi(x,y)}{\partial \nu_x} ds_y. \tag{10}$$

From (9), (10), we have

$$\lim_{\epsilon \to 0} \lim_{h \to 0^+} \int_{\Gamma_{x,\epsilon}} \frac{\partial \Phi(x + h\nu_x, y)}{\partial \nu_x} ds_y = -\frac{1}{2}. \tag{11}$$

.

For the integral on Γ, for any fixed small number $\epsilon > 0$,

$$\begin{aligned} &\lim_{h \to 0^+} \int_{\overline{\Gamma}} \frac{\partial \Phi(x + h\nu_x, y)}{\partial \nu_x} \psi(y) ds_y \\ = &\lim_{h \to 0^+} \int_{\overline{\Gamma} \setminus \Gamma_{x,\epsilon}} \frac{\partial \Phi(x + h\nu_x, y)}{\partial \nu_x} \psi(y) ds_y + \lim_{h \to 0^+} \int_{\Gamma_{x,\epsilon}} \frac{\partial \Phi(x + h\nu_x, y)}{\partial \nu_x} (\psi(y) - \psi(x)) ds_y \\ &+ \lim_{h \to 0^+} \int_{\Gamma_{x,\epsilon}} \frac{\partial \Phi(x + h\nu_x, y)}{\partial \nu_x} ds_y \psi(x) \\ = &\int_{\overline{\Gamma} \setminus \Gamma_{x,\epsilon}} \frac{\partial \Phi(x,y)}{\partial \nu_x} \psi(y) ds_y + \lim_{h \to 0^+} \int_{\Gamma_{x,\epsilon}} \frac{\partial \Phi(x + h\nu_x, y)}{\partial \nu_x} (\psi(y) - \psi(x)) ds_y \\ &+ \lim_{h \to 0^+} \int_{\Gamma_{x,\epsilon}} \frac{\partial \Phi(x + h\nu_x, y)}{\partial \nu_x} ds_y \psi(x). \end{aligned}$$

On the other hand, there exists some constant M that

$$\left| \int_{\Gamma_{x,\epsilon}} \frac{\partial \Phi(x + h\nu_x, y)}{\partial \nu_x} ds_y \right| \leq M$$

and

$$|\psi(y) - \psi(x)| \to 0, \quad \text{as } \epsilon \to 0 \quad \text{for } y \in \Gamma_{x,\epsilon}.$$

Therefore, by letting $\epsilon \to 0$ and noting (11), we obtain

$$\lim_{h\to 0^+} \int_{\overline{\Gamma}} \frac{\partial \Phi(x + h\nu_x, y)}{\partial \nu_x} \psi(y) ds_y = \int_{\overline{\Gamma}} \frac{\partial \Phi(x, y)}{\partial \nu_x} \psi(y) - \frac{1}{2}\psi(x).$$

For $x \in \Gamma$,

$$\lim_{h\to 0^+} \int_{\overline{\Gamma}} \frac{\partial \Phi(x_r + h\nu_x, y)}{\partial \nu_x} \psi(y) ds_y = \int_{\overline{\Gamma}} \frac{\partial \Phi(x_r, y)}{\partial \nu_x} \psi(y).$$

By combining the above, we have

$$\left(\frac{\partial u}{\partial \nu}\right)_+ (x) = \int_{\overline{\Gamma}} \frac{\partial G(x, y)}{\partial \nu_x} \psi(y) ds_y - \frac{1}{2}\psi(x), \quad x \in \Gamma.$$

The proof for $\left(\frac{\partial u}{\partial \nu}\right)_-$ can be carried out in the same fashion.

Appendix B. Plane wave decomposition

The fundamental solution $\tilde{\Phi}(x_1, x_2) = \frac{i}{4} H_0^{(1)}(k\sqrt{x_1^2 + x_2^2})$ solves the equation

$$\Delta \tilde{\Phi} + k^2 \tilde{\Phi} = -\delta(x)$$

in the sense of distribution, where δ is the Dirac mass at the origin. Taking the Fourier transform with respect to x_1 yields

$$\frac{\partial^2 \hat{\tilde{\Phi}}(\kappa, x_2)}{\partial x_2^2} + (k^2 - |\kappa|^2)\hat{\tilde{\Phi}}(\kappa, x_2) = -\delta(x_2).$$

The solution

$$\hat{\tilde{\Phi}}(\kappa, x_2) = \frac{i}{2\sqrt{k^2 - |\kappa|^2}} e^{i\sqrt{k^2 - |\kappa|^2}|x_2|}$$

by noting the radiation condition. The plane wave decomposition is obtained by applying the inverse Fourier transform.

References

[1] H. Ammari, G. Bao, and A.W. Wood, *An integral equation method for the electromagnetic scattering from cavities*, Math. Meth. Appl. Sci. **23** (2000), 1057-1072.

[2] H. Ammari, G. Bao, and A.W. Wood, *Analysis of the electromagnetic scattering from a cavity*, Japan J. Indust. Appl. Math. **19** (2002), 301-310.

[3] H. Ammari, J. Garnier, and K. Sølna, Resolution and stability analysis in full-aperture, linearized conductivity and wave imaging, Proc. Amer. Math. Soc., to appear.

[4] M. Born and E. Wolf, *Principles of Optics* (6th ed.), Cambridge University Press, 1980.

[5] P. Carney and J. Schotland, *Inverse scattering for near-field microscopy*, Appl. Phys. Lett. **77** (2000), 2798-800.

[6] D. Colton and R. Kress, *Integral Equation Methods in Scattering Theory*, Pure and Applied Mathematics, Wiley, New York (1983).

[7] D. Colton and R. Kress, *Inverse Acoustic and Electromagnetic Scattering Theory*, Applied Mathematical Sciences, Vol. 93, Springer-Verlag, Berlin (1998).

[8] D. Courjon and C. Bainier, *Near field microscopy and near field optics*, Rep. Prog. Phys. **57** (1994), 989-1028.

[9] G. Derveaux, G. Papanicolaou and C. Tsogka, *Resolution and denoising in near-field imaging*, Inverse Problems **22** (2006), 1437-1456.

[10] H. W. Engl, M. Hanke, and A. Neubauer, *Regularization of Inverse Problems*, Mathematics and Its Application, Kluwer Academic Pubishers, New York (1996).
[11] L. C. Evans, *Partial Differential Equations*, Graduate Studies in Mathematics, Vol. 19, American Mathematical Society (1997).
[12] A. Kirsch, *An Introduction to the Mathematical Theory of Inverse Problems*, Applied Mathematical Sciences, Vol. 120, Springer-Verlag, New York, 1996.
[13] R. Kress and T. Tran, *Inverse scattering for a locally perturbed half-plane*, Inverse Problems **16** (2000), 1541-1559.
[14] L. Landweber, *An iteration formula for Fredholm integral equations of the first kind*, *Am. J. Math.* **73** (1951), 615-624.
[15] L Novotny and B. Hecht, *Principles of Nano-Optics*, Cambridge University Press (2006).
[16] L. Rayleigh, *On the theory of optical images with special reference to the optical microscope*, Phil. Mag. **5** (1896), 167-195.
[17] F. Reitich and C. Turc, *High-order solutions of three-dimensional roughsurface scattering problems at high-frequencies. I: the scalar case*, Waves Random and Complex Media **15** (2005), 1-16.
[18] J. Sun, P. Carney, and J. Schotland, *Near-field scanning optical tomography: a nondestructive method for three-dimensional nanoscale imaging*, IEEE J. Sel. Top. Quant. **12** (2006), 1072-1082.
[19] A. V. Tikhonov, *On the solution of incorrectly formulated problems and the regularization method*, *Soviet Math. Doklady*, **4** (1963), 1035-1038.
[20] A. Willers, *The Helmholtz equation in disturbed half-spaces,* Math. Meth. Appl. Sci. **9** (1987), 312-323.
[21] B. Zhang and S. N. Chandler-Wilde, *Integral equation methods for scattering by infinite rough surfaces*, Math. Meth. Appl. Sci. **26** (2003), 463-488.

Received November 2011; revised June 2012.

E-mail address: bao@math.msu.edu
E-mail address: linxa011@ima.umn.edu